Dry impregnation in fluidized bed: Drying and calcination effect on nanoparticles dispersion and location in a porous support

Laurie Barthe, Mehrdji Hemati, Karine Philippot, Bruno Chaudret

Dry impregnation in fluidized bed: Drying and calcination effect on nanoparticles dispersion and location in a porous support

L. Barthe [a], *M. Hemati* [a,*], *K. Philippot* [b], *B. Chaudret* [b]

[a] *Laboratoire de Génie Chimique, UMR CNRS 5503, INP-ENSIACET, 5 rue Paulin, Talabot, BP 1301, 31106 Toulouse Cedex 01, France*
[b] *Laboratoire de Chimie de Coordination, UPR CNRS 8241, 205 route de Narbonne, 31077 Toulouse Cedex 04, France*

Keywords:
Metallic nanoparticles
Drying effect
Calcination
Fluidized bed
Porous support

ABSTRACT

The synthesis of metal nanoparticles dispersed inside the grains of a porous inorganic support was carried out by ''dry impregnation'' in a fluidized bed. The principle of this technique consists in the spraying of a solution containing a metal source into a hot fluidized bed of porous particles. The metal source can be of different nature such as metal salts, organometallic precursors or colloidal solutions. The experimental results obtained from iron oxide deposition on a porous silica gel as support, constitute the core of this article but others results concerning the deposition of rhodium from a colloidal suspension containing preformed rhodium nanoparticles are also described. More precisely, this study aims to understand the effect of the bed temperature during the impregnation step, the initial particle porosity and the calcination operating protocol on the metallic nanoparticles dispersion and location in the silica porous particles.

The so-obtained products were characterized by various techniques in order to determine their morphology, their surface properties and the dispersion of the nanoparticles inside the support. The results showed that, under the chosen operating conditions, the deposit efficiency is close to 100% and the competition between the drying rate, depending on the process-related variables, and the capillary penetration rate, depending on the physicochemical-related variables, controls the deposit location. A quasi uniform deposit inside the support particles is observed for soft drying. The metal nanoparticles size is controlled by the pore mean diameter of the support as well as the calcination operating protocol.

1. Introduction

The usual preparation methods of supported catalysts include several steps such as impregnation, filtration, drying and calcination/activation which are realized in different apparatus. The fluidized bed technique is a ''one pot process'' which permits to achieve all the procedure in the same apparatus.

Previous works from our laboratory, concerning impregnation of alumina particles with aqueous solutions of manganese nitrate, showed the feasibility of manufacturing catalysts by direct impregnation of porous support particles through the pulverization of metallic precursor solutions in a hot fluidized bed (Hemati et al., 2003; Desportes et al., 2005). From these results it appeared that, according to the operation conditions, the pulverization of a metallic salt aqueous solution on porous particles can lead to two cases:

- in conditions favoring a fast solvent evaporation, a deposit on the external surface of the support takes place;
- in conditions of soft drying, an homogenous impregnation is available.

* *Corresponding author.*
E-mail address: Mehrdji.Hemati@ensiacet.fr (M. Hemati).

Nomenclature

c_l	precursor concentration in the solution (kg/kg of solvent)
d_p	particle mean diameter (m)
d_{pore}	pore mean diameter (m)
l	pore length (m)
m_s	initial weight of solid particles (kg)
$\dot{m}_{so}$	solvent mass flow rate (kg/s)
r_{pore}	pore radius (m)
S_{BET}	specific area (m^2/g)
t	operation time (s)
t_{cap}	wetting time or capillary penetration time (s)
t_{sec}	drying time (s)
T_{bed}	bed temperature (K)
U_{mf}	minimal fluidization velocity (at 25 °C) (m/s)
U_t	terminal velocity (at 25 °C) (m/s)
V_p	pore volume (m^3/g)

Greek letters

β	heating rate (°C/min)
γ_{LV}	liquid–gas interfacial tension ($N\,m^{-1}$)
θ	contact angle (rad)
μ	liquid viscosity (Pa s)
τ_{real}	experimental deposit rate (%)
τ_{theo}	theoretical deposit rate (%)
χ	internal porosity (%)

In addition, it was highlighted that for the treatment of coarse porous particles ($d_p > 1500\ \mu m$), the precursor distribution inside the particles depends on two characteristic times:

- the time necessary for the liquid penetration in the pores, t_{cap}. It can be estimated from the following equation taken from the model of the parallel capillary beam:

$$t_{cap} = \frac{2\mu l^2}{\gamma_{LV} \cos\theta r_{pore}} \quad (1)$$

  where μ is the liquid viscosity, l the pore length equivalent to the particle radius multiplied by the tortuosity factor, γ_{LV} the interfacial tension, θ the contact angle and r_{pore} is the pore radius;
- the drying time, t_{sec}, defined as the time necessary for a particle saturated by pure solvent to be transformed into a dry particle under fluidized bed conditions (temperature and humidity). The calculation of this characteristic time is based on the mass and energy balances on a single wetted particle considering that the mass transfer is controlled by external resistance (gas phase). The model's equations were described in a previous publication (Barthe et al., 2007; Desportes, 2005).

The solute distribution can be considered as uniform when the ratio between these two characteristic times becomes higher than 10 (Desportes et al., 2005).

This study deals with the preparation of iron oxide nanoparticles within fine porous silica particles (<150 μm). In addition to the process parameters which affect the metal precursor distribution in the porous support, the influence of the support porosity and of calcination operating conditions on the iron oxide nanoparticles location and dispersion were studied. Finally, during dry impregnation of silica gel with a rhodium colloidal suspension, the effect of the bed temperature on the dispersion and location of rhodium nanoparticles in a silica gel is described.

2. Methods and materials

2.1. Experimental set-up

The experiments were carried out in a batch fluidized bed. The reactor is a stainless steel conical column with a 30 mm base diameter, a 112 mm top diameter and 300 mm in height (Fig. 1). Its dimensions make possible to reduce the metal precursor consumption and the impregnation time since it operates at laboratory scale (production of catalyst: 30–100 g).

In order to check the representativeness of the results obtained in this pilot, a series of experiments was carried out in a fluidized bed with a 100 mm diameter column, allowing to treat a support mass of 3 kg. The confrontation of the results obtained in the two pilots, in similar operating conditions, led to identical conclusions.

The gas distribution at the column base is ensured by a stainless steel perforated plate with a porosity of 0.5% (12 holes of 1 mm, organized according to a triangular mesh of 5 mm). Before entering the bed, the fluidizing gas flow rate is measured by a rotameter and preheated by an electrical heater. The bed temperature is controlled by means of a PID regulator which commands the furnace heating power. At the outlet of the column, the elutriated particles are separated from the gas phase by a cyclone.

The impregnating solutions are placed into two reservoirs, one containing pure solvent for experiment starting, and the second containing the metallic precursor solution. The solution is drawn up by a volumetric pump from a reservoir to a spray nozzle. The atomizer is a downward facing nozzle and is located in the bed. In previous works (Cherif, 1994; Hemati et al., 2003) the influence of the nozzle position was examined during fluidized bed coating and granulation. The experimental results showed that the most appropriate position of the atomizing nozzle was when the tip of the nozzle coincided with the surface of the packed bed and thus became submerged when the bed was fluidized. This permitted to avoid the formation of a cake (called also "*caking*") and to maintain a stable operation with maximum

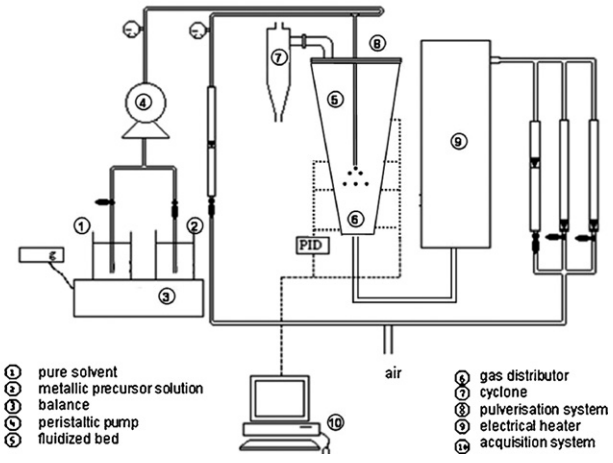

Fig. 1 – Experimental set-up.

efficiency. Temperature and pressure drop monitoring is achieved throughout all the impregnation.

The general experimental protocol is as follows:

- The column is initially charged with a given mass of porous particles.
- The powder is fluidized by a fixed hot gas flow rate.
- The pure solvent is sprayed within the bed, at the same flow rate as the metallic precursor solution.
- As soon as the thermal steady state regime is reached, the solvent is replaced by the solution containing metallic precursor. Solid samples can be taken at different times to follow the impregnation kinetics.
- At the end of the impregnation step, the decomposition/activation of the precursor is carried out by stopping spraying and by increasing the bed temperature. Thus, nanoparticles of metal oxide are obtained through samples calcination under air. It is important to note, that when a colloidal suspension is sprayed, no further treatment is necessary since the deposit obtained after the impregnation is directly constituted of metallic nanoparticles.

2.2. Supports and metal sources

2.2.1. Solid supports

The experiments were carried out with three silica gels. These solids have almost the same size but are different by their porosity and specific surface. Their pore diameters vary from 14 to 3 nm. Their physical and hydrodynamic properties are reported in Table 1.

2.2.2. Metal source

To obtain iron based composite materials, the solution used as the metal source during the impregnation step, is an aqueous solution of iron nitrate $Fe(NO_3)_3{\cdot}9H_2O$ (33 mass%). This compound has a monoclinic crystalline structure and is very water soluble (saturation concentration at 25 °C: 300 g of crystals/100 g of water). Its melting point is about 47 °C and it loses some water constitution molecules between 60 and 160 °C. Its decomposition at a temperature greater than 200 °C leads to the formation of iron oxide Fe_2O_3. Other properties of this precursor were determined such as its viscosity (3.54×10^{-3} Pa s), its superficial tension (75.1 mN m^{-1}) and its contact angle (54°).

The rhodium colloidal aqueous suspensions containing rhodium (0) colloids were prepared as previously described by Roucoux et al. (2000).

More precisely, sodium borohydride was added to an aqueous solution containing the surfactant HEA16Cl (*N*,*N*-dimethyl-*N*-cetyl-*N*-(2-hydroxyethyl)ammonium salts). This solution was quickly added under vigorous stirring to an aqueous solution of the precursor $RhCl_3$, $3H_2O$. The initial red solution darkened immediately attesting of the obtaining of an aqueous Rh^0 colloidal suspension which remains stable for a long time. The average rhodium particles size is around 2.4 nm.

Table 1 – Physical and hydrodynamic properties of silica gels

Properties	Silica 1	Silica 2	Silica 3
Mean diameter, d_p (μm)	130	130	120
Pore diameter, d_{pore} (nm)	14	5.5	3
Specific surfaces, S_{bet} (m^2/g)	320	530	790
Pore volume, V_p (cm^3/g)	1.08	0.81	0.15
Internal porosity, χ (%)	70	60	30
U_{mf} at 25 °C (minimum fluidization velocity) (m/s)	0.003	0.0035	0.006
U_t at 25 °C (terminal velocity) (m/s)	0.18	0.23	0.38

2.3. Characterization methods

The textural properties of the samples were characterized using different techniques:

- Particles mean diameter and size distribution were estimated by laser granulometry.
- Samples specific surfaces and pore size distributions were determined by the BET standard method (N_2 adsorption–desorption).
- Apparent and skeletal densities were obtained with helium pycnometry and pore volume with mercury porosimetry.
- After calcination, the silica gel particles morphology was studied by scanning electron microscopy (SEM). The topology and the size of metal nanoparticles were analyzed by transmission electron microscopy (TEM). Chemical detection of the element was obtained by chemical element detector (XRD) coupled with SEM. This information permits to understand the surface morphology and the chemical element distribution on the solid cross sectional.
- Precursor solution viscosity was estimated by a rheometer and its superficial tension was measured according to the Wilhelmy principle. The contact angle was determined using capillary rise method exploiting the results with Washburn relationship.
- Metal loading of composite materials was determined by elemental analysis.

From metal contents measurements by elemental analysis, the experimental impregnation rate, τ_{real}, can be estimated. It is defined by the ratio between the precursor mass really deposited and the virgin support mass.

A theoretical impregnation rate, τ_{theo}, is also defined as the ratio between the quantity of precursor sprayed during a time t and the mass of virgin support present in the fluidized bed:

$$\tau_{theo} = 100\frac{\dot{m}_{so} c_l t}{m_s} \quad (2)$$

where $\dot{m}_{so}$ is the solution mass flow rate, c_l the precursor concentration, t the operation time, and m_s is the initial mass of solid particles in the bed. These rates are expressed in percentages.

An impregnation efficiency is calculated, considering the ratio between the experimental impregnation rate (τ_{real}) and the theoretical impregnation rate (τ_{theo}):

$$\text{efficiency} = \frac{\tau_{real}}{\tau_{theo}} \quad (3)$$

2.4. Experiments

For all the experiments carried out, the solution flow rate (50 g/h), the fluidization gas flow rate (0.96 kg/h) and the support mass (30 g) were maintained constant. It should be noted that the selected gas flow rate is about 10 times the minimum fluidization velocity at 25 °C. For every experiment,

Table 2 – Experiments carried out with iron nitrate solution and with rhodium colloidal suspension					
Experiment number	Support specific surfaces, S_{bet} (m^2/g)	Bed temperature, T_{bed} (°C)	Impregnation rate (%)	Final metal loading (%)	t_{sec}/t_{cap} (–)
Precursor: iron nitrate solution					
1	530	64	5.2	0.7	80
2	530	64	15.4	2	80
3	530	64	29.9	4	80
4	320	66	29.6	4	80
5	790	68	29.7	4	80
6	530	46	30.0	4	400
7	530	86	30.1	4	40
Precursor: rhodium colloidal suspension					
8	530	45	–	0.1	400
9	530	116	–	0.1	8

the final metal loading and the t_{sec}/t_{cap} ratio are already presented.

In Table 2 the list of experiments carried out is reported. Experiments 1 to 7 concern iron based materials. The impregnation kinetics can be studied from experiments 1 to 3. The effect of process parameter, bed temperature, on the metal precursor dispersion in the porous support can be examined by taking into account experiments 3, 6 and 7 while the porosity effect can be observed analyzing experiments 3 to 5.

Table 2 also contains the experiments 8 and 9 related to rhodium catalysts. The operating conditions were chosen to study the bed temperature effect on the deposit location. It should be noted that in the case of rhodium, only one silica gel was used with a specific surface of 530 m^2/g (silica 2).

3. Results and discussion

3.1. *Impregnation kinetics*

Experiments 1, 2 and 3 (Table 2), were performed under the same operating conditions but with different operation times leading to different impregnation rates, in the case of iron samples. Their analysis makes it possible to better understand the product texture and structure evolution during the treatment. The conclusions drawn from this example can be generalized to the most part of the experiments.

Fig. 2 shows the evolution of the theoretical and the experimental impregnation rates versus impregnation times. These data are given with an estimated uncertainty of 5%.

This graph shows that, the two impregnation rates are very close and vary linearly during the pulverization. It also indicates that the deposit effectiveness is close to 100%, and

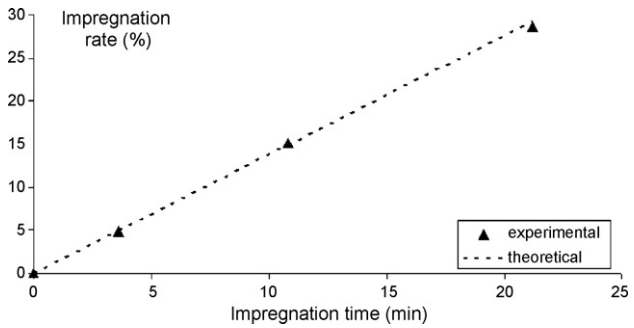

Fig. 2 – Impregnation rates vs. pulverization time (impregnation kinetics: experiments 1 to 3).

that there is no loss of precursor. At a given precursor concentration, the spraying time determines the metal loading for each experiment.

The granulometry analysis reveals that the particles size distribution and the particles mean diameter (d_{50}) remain unchanged during the operation (Fig. 3). Thus, there is no increase of the particles size, nor an agglomeration phenomenon.

Figs. 4 and 5 present respectively the evolution of the pore size distribution for different impregnation rates, and the influence of the impregnation rate on the catalyst specific surface and pore volume.

It can be observed that the pore size distribution pattern is not modified during the impregnation. Moreover, the pore volume and of the specific surface evolve linearly during the treatment. These results indicate that the deposit is performed inside the pores of the silica gel.

3.2. *Calcination*

For iron based composite materials, the deposit morphology was observed after the calcination step under air for samples containing 4% of iron. Let us note that for iron contents lower or equal to 2%, the micrographs analysis is difficult because of the weak contrast between the chemical elements.

The impregnated solids, obtained from experiment 3, were treated at two temperatures: 450 and 900 °C. Table 3 shows the calcination protocols which were followed, depending on the heating rate, β. Quasi instantaneous calcinations were carried out by putting a small quantity of the product in a fluidized bed (Barthe, 2007) previously planned at the desired temperature. The other calcinations were carried out in a muffle furnace at programmable heating rates. The resulting materials were analyzed by TEM after a preparation by ultramicrotomy. It should be noted that the observation of various TEM micrographs showed a quasi homogeneous dispersion of the nanoparticles inside the silica porous particles.

Table 3 also gathers the average size of the nanoparticles obtained according to the conditions of calcination.

The results evidence that, whatever the temperature reached, the heating rate has a notable effect on the nanoparticles and/or clusters size. A heating rate decrease leads to a reduction of the clusters size and even to their disappearance, Table 3 and Figs. 6 and 7.

In addition, in the case of a calcination treatment at 450 °C and $\beta = 7$, the size distribution reveals two different populations of clusters respectively centered at 6 and 15 nm. To explain this observation, it is necessary to establish two essential concepts.

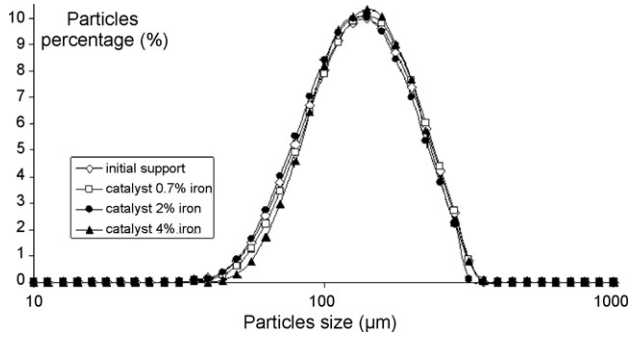

Fig. 3 – Evolution of the particles size distribution during the impregnation (impregnation kinetics: experiments 1 to 3).

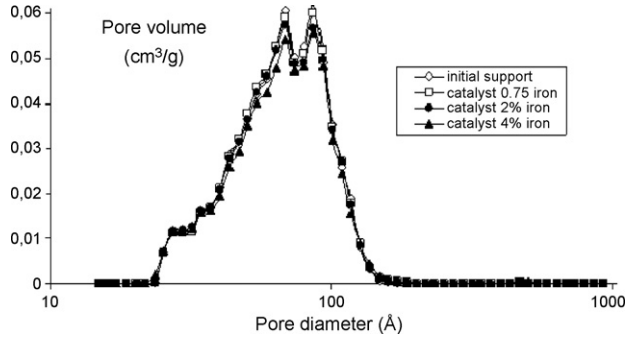

Fig. 4 – Evolution of the catalyst pore size distribution during impregnation (impregnation kinetics: experiments 1 to 3).

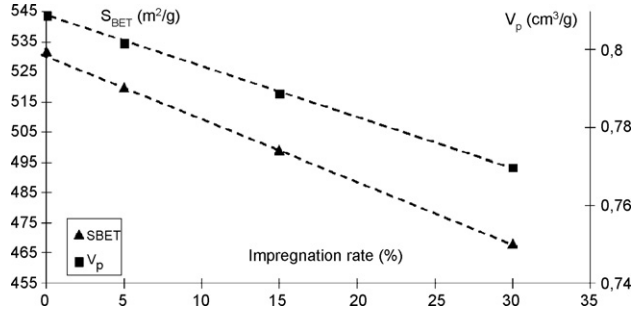

Fig. 5 – Catalyst specific surface and pore volume vs. impregnation rate (impregnation kinetics: experiments 1 to 3).

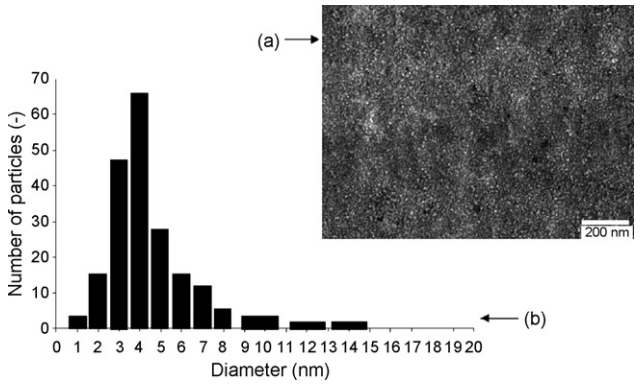

Fig. 6 – Iron based catalysts treated at 450 °C and β = 0.3: (a) TEM micrograph; (b) nanoparticles size distribution (calcination effect: experiment 3).

Firstly, the silica gel morphology can be represented by a structure of the pellet-grain type (Barby, 1976), including two porosity types (Fig. 8):

- microporosity and mesoporosity on the level of the elementary grain;
- mesoporosity and macroporosity in the intergranular space.

During impregnation, due to strong capillary tensions existing at the level of the elementary grains (low pore diameters), the aqueous solution tends to penetrate inside them. Once the elementary grains are saturated, the deposit can take place in the intergranular spaces. We can thus suppose that the privileged place for the clusters formation is in the intergranular space, while individual nanoparticles are formed in the elementary grains.

Moreover, during calcination, the deposited crystals undergo several transformations: melting at 45 °C, water constitution molecules loss between 60 and 120 °C and decomposition beyond 200 °C. It should be noted that the first two stages are strongly endothermic and thus require an important energy contribution.

At low heating rate, the transformation phenomena (melting and drying) are very slow. So the precursor migration can homogenize its dispersion inside the pores. The deposit privileged place is the elementary grain. Then the pore diameter control the nanoparticles maximum size, which leads to the formation of individual nanoparticles of 5 nm, distributed in a uniform way in the porous matrix (Table 3, Fig. 6a and b).

Concerning the products obtained by fast calcination, two types of morphology are detected: nanoparticles agglomerates (clusters) and individual nanoparticles (Fig. 7a and b). This phenomenon can be explained by a heating rate effect on the temperature range corresponding to the various precursor transformations (melting, constitution water elimination and

Table 3 – Average size of nanoparticles or clusters observed according to the calcination protocol (calcination effect: experiment 3)

Temperature reached (°C)	Duration of temperature rise (h)	Heating rate, β (°C/min)	Average size of nanoparticles or clusters observed (nm)
450	24	0.3	5 ± 0.5
450	1	7	13 ± 7
450	Instantaneous	>5000	30 ± 20
900	24	0.6	5 ± 0.5
900	1.75	8	10 ± 5
900	Instantaneous	>5000	15 ± 10

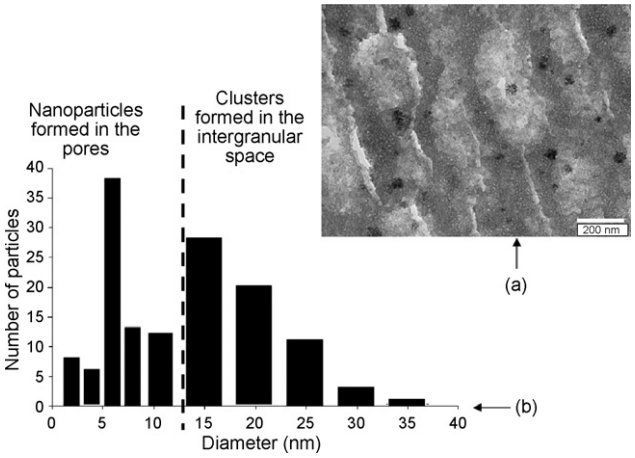

Fig. 7 – Iron based catalysts treated at 450 °C and β = 7: (a) TEM micrograph; (b) nanoparticles size distribution (calcination effect: experiment 3).

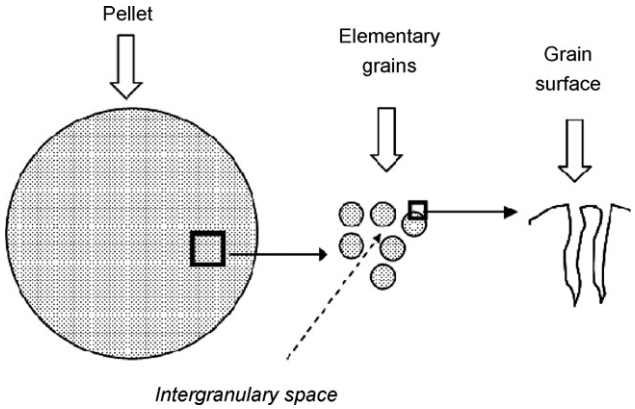

Fig. 8 – Schematic representation of a silica particle according to the pellet-grain model.

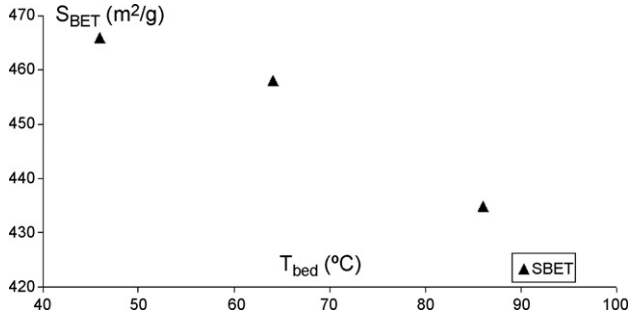

Fig. 9 – Specific surface vs. bed temperature (process parameters effect: experiments 3, 6 and 7).

Table 4 – Iron loading (%) determined at various areas of silica particles: (a) t_{sec}/t_{cap} of 400 (T_{bed} 46 °C); (b) t_{sec}/t_{cap} of 40 (T_{bed} 86 °C) (process parameters effect: experiments 6 and 7)

Border	Intermediate zone	Center
(a) t_{sec}/t_{cap} of 400 (T_{bed} 46 °C)		
4.4	3.1	3.4
4.0	3.7	3.4
3.8	4.3	4.2
3.8	4.4	3.9

Border	Intermediate border zone	Intermediate center zone	Center
(b) t_{sec}/t_{cap} of 40 (T_{bed} 86 °C)			
6.5	4.9	3.8	2.3
4.6	3.2	2.1	1.8
4.3	2.9	2.6	2.8

decomposition). Indeed, these temperature ranges are moved towards higher temperatures when the heating rate is increased. Thus, the internal tension due to the temperature rise can involve the expulsion of some precursor from the elementary grains of the silica particles towards interstitial spaces and clusters formation. These phenomena explain the existence of a bimodal distribution in Fig. 7a and b.

Thereafter, with the objective to favor the formation of easily observable Fe_2O_3 nanoparticles clusters, all the samples were calcined at 450 °C, keeping a heating rate of 7 °C/min.

3.3. *Effect of the process parameters*

The process parameters which can affect the impregnation operation are:

- the fluidized bed temperature;
- the fluidization gas flow rate;
- the precursor liquid flow rate.

The choice of the liquid and gas flow rates depends on the constraints related on one hand to the fluidization quality (solid mixing, elutriation phenomenon) and on the other hand to the maximum evaporative rate of the apparatus (heating power). Preliminary tests allowed to fix their values at 0.8 m^3/h for the gas flow rate and 50 g/h for the liquid flow rate. The only parameter which can easily be varied on the installation is the bed temperature, T_{bed}. It was modified, for iron catalysts, between 46 and 86 °C corresponding to a value of the ratio t_{sec}/t_{cap} between 400 and 40 (experiments 3, 6 and 7).

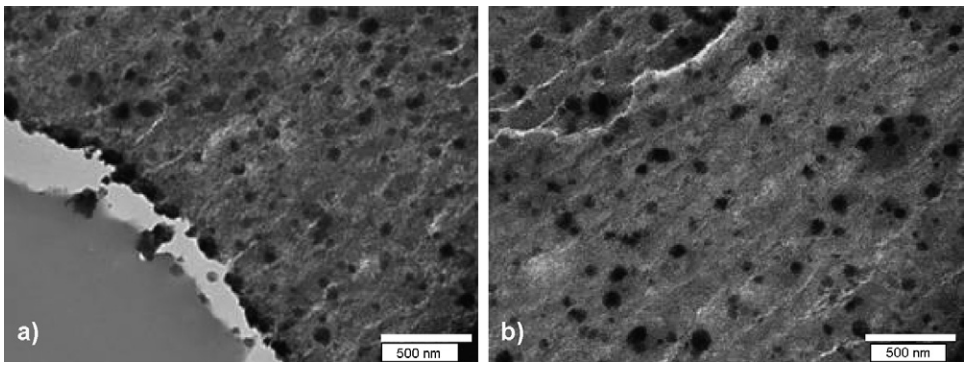

Fig. 10 – Micrographs of calcined sample (a) at the particle surface, (b) in the particle center (process parameters effect: experiments 6, t_{sec}/t_{cap} = 400).

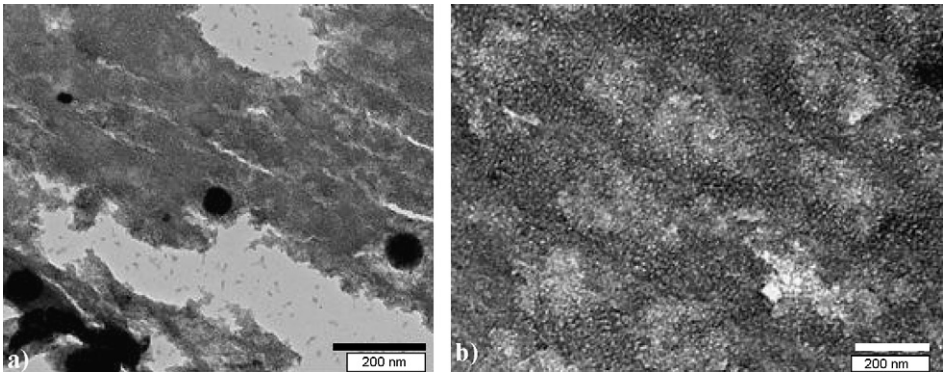

Fig. 11 – Micrographs of calcined samples (a) at the particle surface, (b) in the particle center (process parameters effect: experiments 7, t_{sec}/t_{cap} = 40).

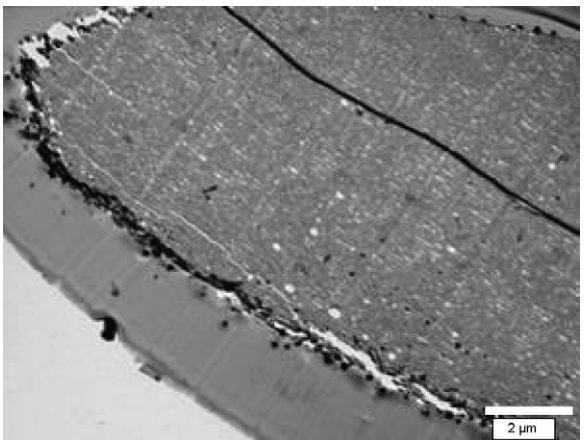

Fig. 12 – Micrograph of a particle from the calcined sample (process parameters effect: experiments 7, t_{sec}/t_{cap} = 40).

3.3.1. Iron based catalysts

It can be deduced from Fig. 9 that an increase of the bed temperature (reduction of t_{sec}/t_{cap}) leads to a decrease of the specific surface. This phenomenon is more important at temperature higher than 60 °C.

To better understand the effect of this parameter on the iron oxide nanoparticles distribution in the silica grains, several cuts of particles of each sample were observed by SEM coupled to XRD, in order to estimate the iron loading in the various areas of the silica particles: border, intermediate zone and center (Table 4a and b).

The results show that, for a high t_{sec}/t_{cap} ratio (400), the deposit is performed inside the particles and that the iron loading is quasi uniform in the entire volume of the particles. When the t_{sec}/t_{cap} ratio decreases to a threshold value of 10 (case of t_{sec}/t_{cap} of 40), an iron gradient from the center towards the surface of the particles is observed.

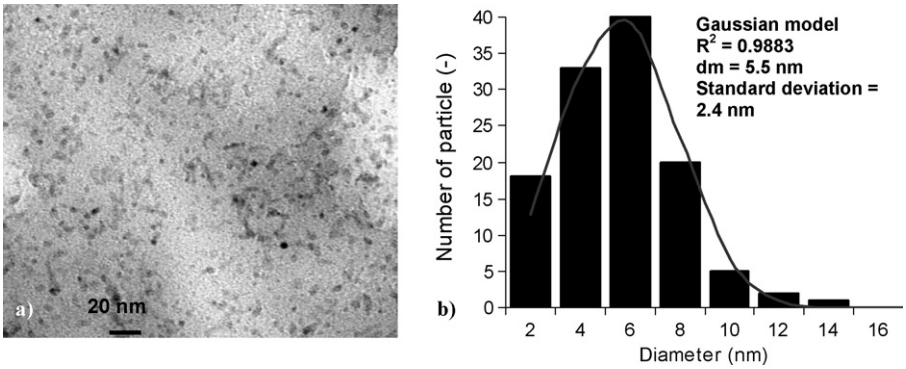

Fig. 13 – Effect of bed temperature on rhodium nanoparticles location and morphologies: (a) TEM micrograph; (b) nanoparticles size distribution (process parameters effect: experiments 8, t_{sec}/t_{cap} = 60).

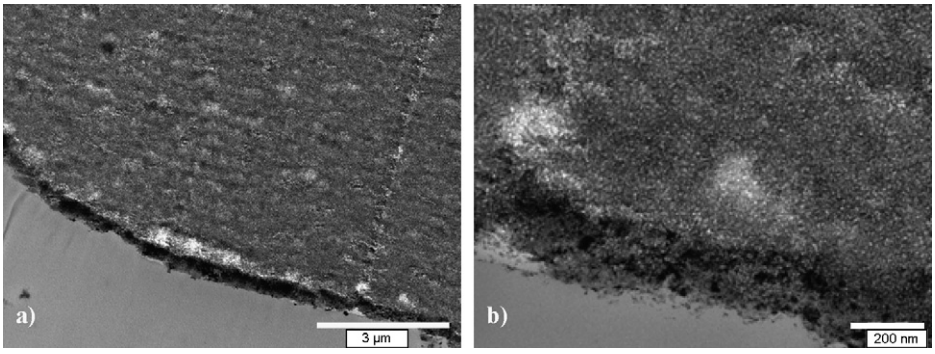

Fig. 14 – Effect of the bed temperature on rhodium nanoparticles location and morphologies: (a) TEM micrograph (scale 20 000); (b) TEM micrograph scale (100 000) (process parameters effect: experiments 9, t_{sec}/t_{cap} = 3).

The TEM analysis after ultramicrotomy confirms the previous results. When t_{sec}/t_{cap} is rather high (400), the clusters are spread out uniformly in the particles (Fig. 10).

For a low value of t_{sec}/t_{cap} ($\leq$40), the samples display many clusters at the surface but individual nanoparticles in the core of the silica particles (Fig. 11). This observation was confirmed by TEM analysis at lower magnification showing that Fe_2O_3 clusters are located at the silica particles border (Fig. 12).

In summary, the choice of the bed temperature and thus the t_{sec}/t_{cap} ratio is a key parameter of the process since it makes it possible to control the deposit location inside the support grains during the impregnation step.

3.3.2. *Rhodium based catalysts*

The effect of the process parameters on the active element location was also studied in the case of materials obtained by spraying a rhodium colloidal suspension containing preformed nanoparticles. Two experiments were performed (Table 2, experiments 8 and 9) to observe the influence of the bed temperature (and so t_{sec}/t_{cap} ratio) on deposited nanoparticles location. The objective was to deposit uniformly the metal inside the porous support during experiment 8 and at the surface of the silica gel during experiment 9.

As observed by TEM, a homogeneous deposit is obtained throughout the support particles when the t_{sec}/t_{cap} ratio is about 400 (Fig. 13a). After deposition, the rhodium nanoparticles have an average size of around 5 nm corresponding to the pore average diameter (Fig. 13b).

When the t_{sec}/t_{cap} ratio is around 8, a surface deposit is observed, like a surface coating (Fig. 14a). The thickness of the formed coat is approximately about 200 nm and is composed by individual nanoparticles clusters (20–30 nm) (Fig. 14b).

These results demonstrate that, whatever the support diameter (coarse or fine), or the precursor nature (metal salts,

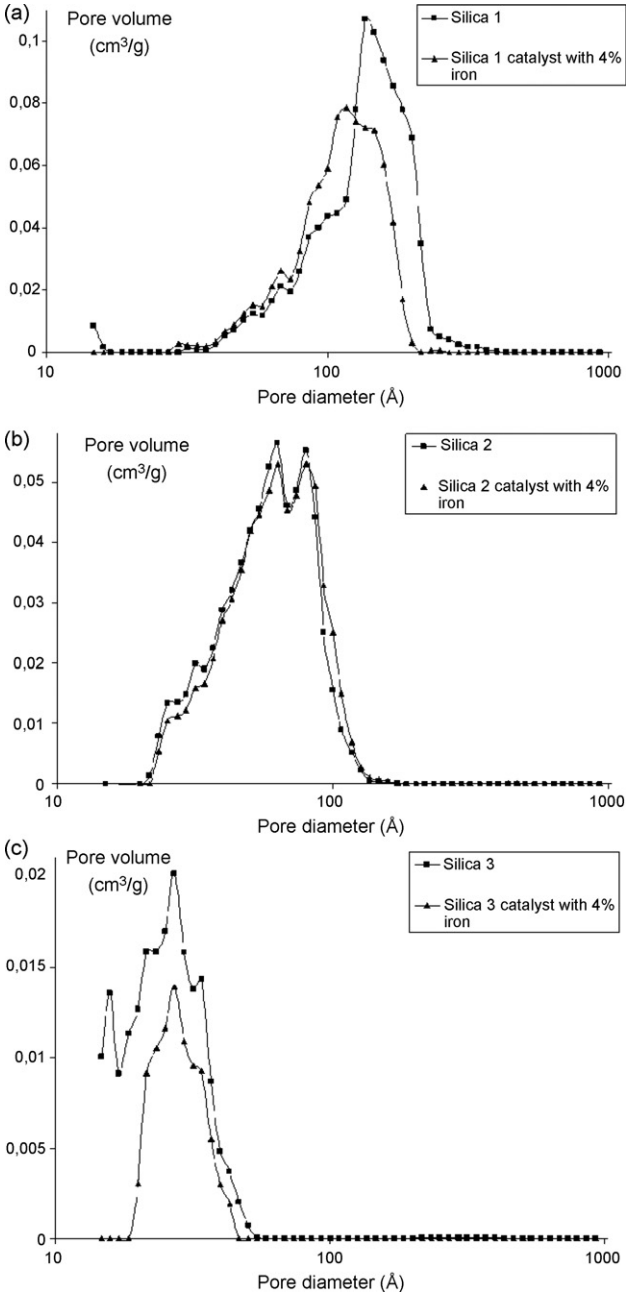

Fig. 15 – Pore size distribution of the virgin support and the calcined catalyst according to the silica: (a) silica 1; (b) silica 2; (c) silica 3 (support physical properties effect: experiments 3 to 5).

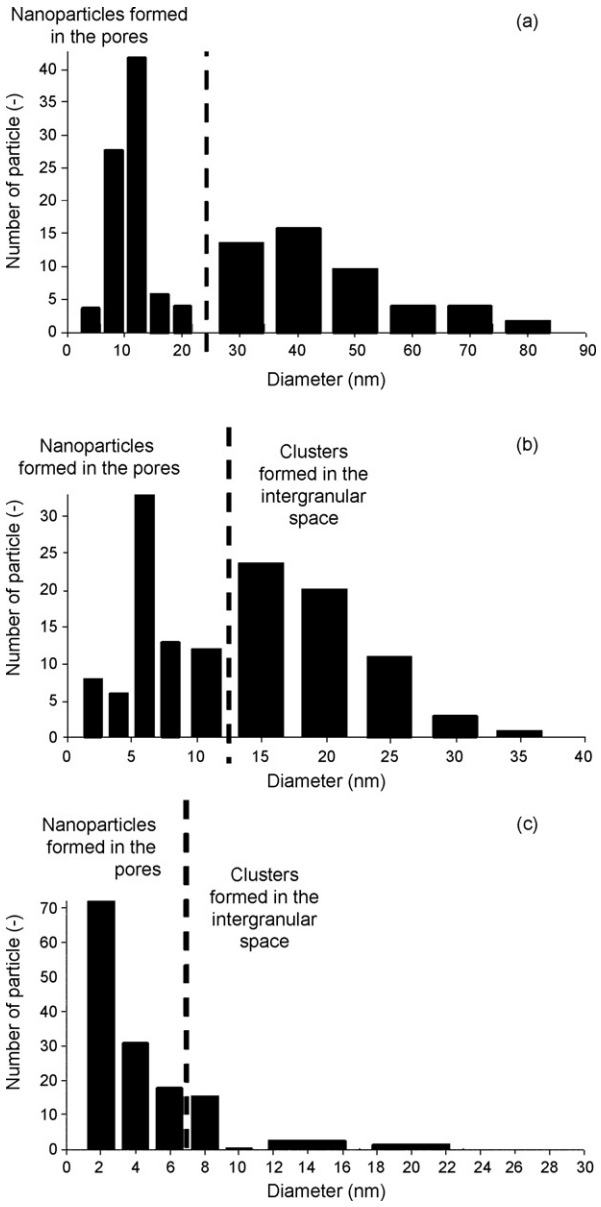

Fig. 16 – Nanoparticles size distribution according to the support porosity after calcination: (a) silica 1; (b) silica 2; (c) silica 3 (support physical properties effect: experiments 3 to 5).

Table 5 – Porosity of initial support and impregnated products and nanoparticles size obtained (support physical properties effect: experiments 3 to 5

	Silica 1		Silica 2		Silica 3	
	(V)	(+Fe)	(V)	(+Fe)	(V)	(+Fe)
Pore diameter, d_p (nm)	14	11	5.5	5.7	3	3
Specific area, S_{bet} (m^2/g)	320	317	530	467	790	599
Pore volume, V_p (cm^3/g)	1.08	0.90	0.81	0.77	0.15	0.10
Average nanoparticle sizes (nm)		21		13		4

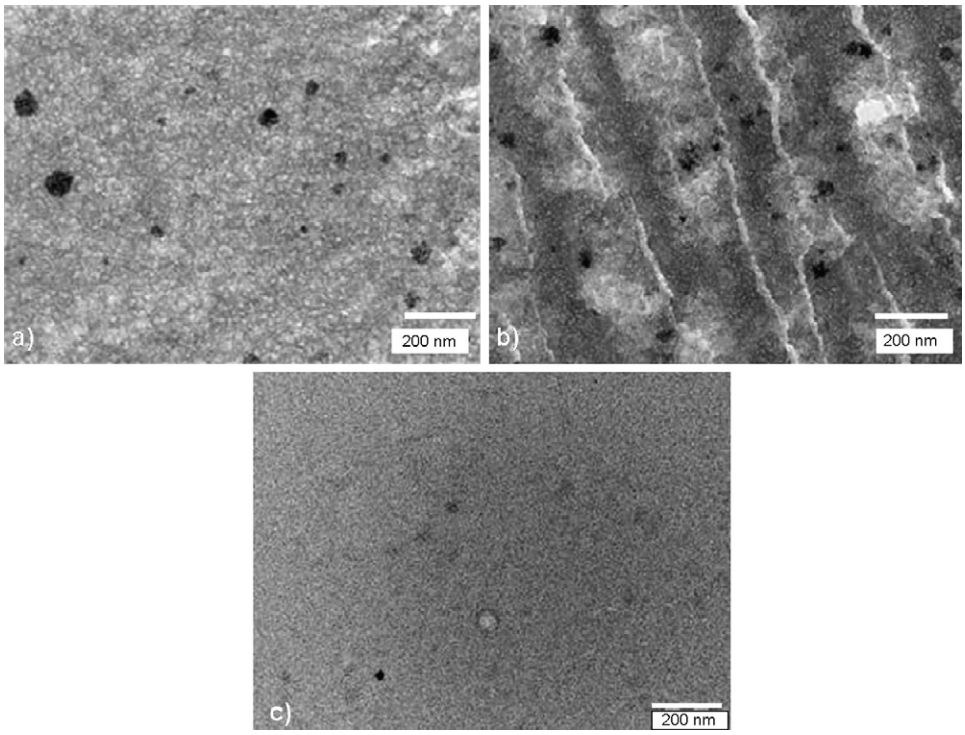

Fig. 17 – TEM micrographs of iron based catalysts: (a) silica 1; (b) silica 2; (c) silica 3 (support physical properties effect: experiments 3 to 5).

colloidal suspensions or even an organometallic complex Desportes et al., 2005), by fixing the operating conditions, the deposit location can be oriented.

3.4. *Effect of the support porosity*

The effect of the support physical properties was examined by spraying iron nitrate on silica gels having different porosities (experiments 3 to 5). The operating conditions correspond to a soft drying, sustaining a uniform deposit inside the supports particles. Chosen calcination conditions were the following: temperature = 450 °C; heating rate = 7 °C/min. The objective is to favor the formation of easily observable Fe_2O_3 nanoparticles clusters.

In Table 5 are reported the results of BET analysis for the virgin supports (V) and the calcined samples (+Fe) and the nanoparticles sizes obtained.

It appears that the evolution of the pore size distribution, the pore volume and the specific surface, indicate a deposit taking place mainly in the support whatever the silica. The global pore size distribution pattern is always conserved (Fig. 15a–c).

This was confirmed by TEM observation carried out in various areas of the silica particles. All the samples present the same uniform nanoparticles distribution.

Moreover, the cluster average size decreases when the average pore diameter decreases. Indeed, the deposit takes place inside the pores due to the value of $t_{sec}/t_{cap} \geq 10$. But as explained in Section 2, the chosen calcination conditions favor the formation of two types of nanoparticles morphology: clusters in the intergranular space and individual nanoparticles in the pore. The bimodal nanoparticles size distributions, presented in Figs. 16 and 17, confirm these observations. So these results let think that the pores diameter controls the clusters maximum size formed inside the pores.

4. Conclusion

The synthesis and the characterization of iron based materials obtained by dry impregnation in a fluidized bed from the pulverization of iron nitrate solutions on various silica gels were described. The operation effectiveness is 100%. The results show that depending on the operating conditions, the deposit location can be controlled and this in a quasi uniform way. Under our operating conditions, the calcination protocol plays an important role in the precursor redistribution during the stage of nanoparticles formation. Moreover, the nanoparticles cluster size could depend on support pore size.

The deposit location can also be controlled even using a colloidal suspension containing preformed nanoparticles as metal source.

Composite materials so-obtained have been tested as catalysts: iron catalysts in carbon nanotubes synthesis and rhodium catalysts for aromatic hydrogenation. The composite materials prepared by such a dry impregnation with a metallic salt or with a colloidal suspension present good activities and selectivity in the studied reaction.

Dry impregnation in a fluidized bed proves to be a powerful technique whose most outstanding advantages are composite materials preparation in a single apparatus, and the possibility of controlling the deposit location by the choice of the operating conditions.

REFERENCES

Barby, D. 1976, In G. D. Parfitt & K. S. W. Sing (Eds.), Characterization of Powder Surfaces (pp. 353–). London: Academic Press.

Barthe, L., 2007, Synthèse et dépôt de nanoparticules métalliques dans un support poreux par imprégnation en voie sèche dans un lit fluidisé: élaboration de catalyseurs supportés, PhD thesis, INP Toulouse.

Barthe, L., Desportes, S., Hemati, M., Philippot, K. and Chaudret, B., 2007, Synthesis of supported catalysts by dry impregnation in fluidized bed, Chem Eng Res Des, 85(A6): 1–11.

Cherif, R., 1994, Contribution à l'étude d'enrobage des particules solides en lit fluidisé, PhD thesis, INP Toulouse.

Desportes, S., 2005, Imprégnation en voie sèche en lit fluidisé, application à la synthèse de catalyseurs supportés, PhD thesis, INP Toulouse.

Desportes, S., Steinmetz, D., Hemati, M., Philippot, K. and Chaudret, B., 2005, Production of supported asymmetric catalysis in a fluidized bed, Powder Technol, 157: 12–19.

Hemati, M., Cherif, R., Saleh, K. and Pont, V., 2003, Fluidized bed coating and granulation: influence of process-related variables and physicochemical properties on the growth kinetics, Powder Technol, 130: 18–34.

Roucoux, A., Schulz, J. and Patin, H., 2000, Stabilized rhodium (o) nanoparticles: a reusable hydrogenation catalyst for arene derivatives in a biphasic water–liquid system, Chem Eur J, 6(No. 4): 618–624.